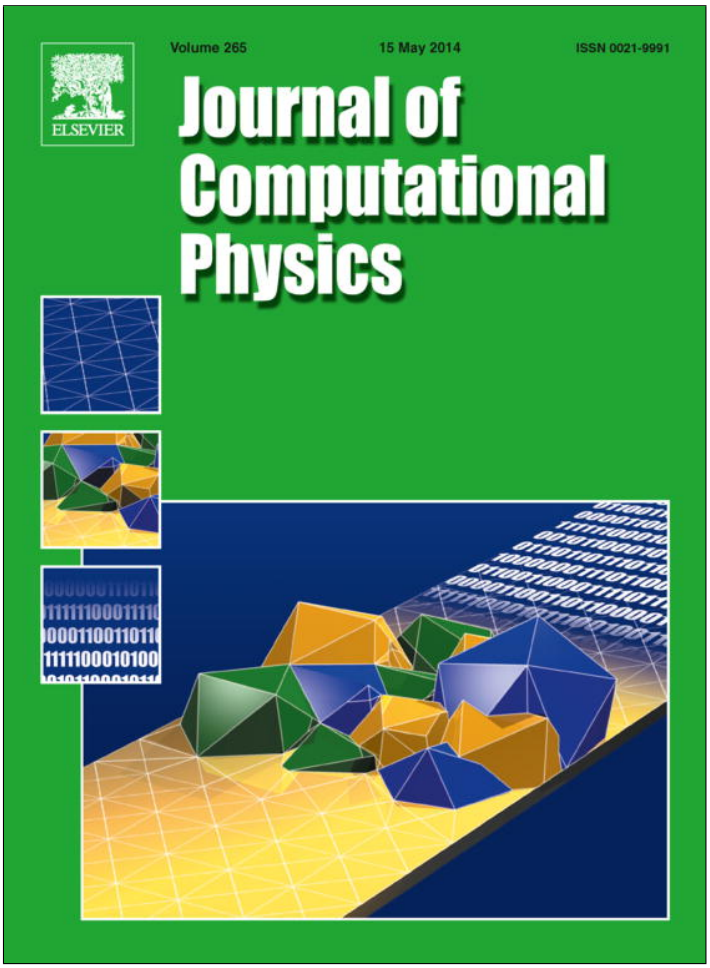

Journal of Computational Physics 265 (2014) 113–127

Contents lists available at ScienceDirect

Journal of Computational Physics

www.elsevier.com/locate/jcp

Energy-conserving dissipative particle dynamics with temperature-dependent properties

Zhen Li [a], Yu-Hang Tang [a], Huan Lei [b], Bruce Caswell [c], George Em Karniadakis [a,*]

[a] Division of Applied Mathematics, Brown University, Providence, RI 02912, USA
[b] Pacific Northwest National Laboratory, Richland, WA 99352, USA
[c] School of Engineering, Brown University, Providence, RI 02912, USA

ARTICLE INFO

Article history:
Received 29 August 2013
Received in revised form 10 December 2013
Accepted 3 February 2014
Available online 10 February 2014

Keywords:
DPD
Thermal boundary condition
Thermal conductivity
Variable properties
Mesoscopic dynamics

ABSTRACT

The dynamic properties of fluid, including diffusivity and viscosity, are temperature-dependent and can significantly influence the flow dynamics of mesoscopic non-isothermal systems. To capture the correct temperature-dependence of a fluid, an energy-conserving dissipative particle dynamics (eDPD) model is developed by expressing the weighting terms of the dissipative force and the random force as functions of temperature. The diffusivity and viscosity of liquid water at various temperatures ranging from 273 K to 373 K are used as examples for verifying the proposed model. Simulations of a Poiseuille flow and a steady case of heat conduction for reproducing the Fourier law are carried out to validate the present eDPD formulation and the thermal boundary conditions. Results show that the present eDPD model recovers the standard DPD model when isothermal fluid systems are considered. For non-isothermal fluid systems, the present model can predict the diffusivity and viscosity consistent with available experimental data of liquid water at various temperatures. Moreover, an analytical formula for determining the mesoscopic heat friction is proposed. The validity of the formula is confirmed by reproducing the experimental data for Prandtl number of liquid water at various temperatures. The proposed method is demonstrated in water but it can be readily extended to other liquids.

1. Introduction

Dissipative particle dynamics (DPD) is a particle-based method introduced by Hoogerbrugge and Koelman [1] for performing mesoscopic simulations of complex fluids. Initially, DPD was designed to have the advantages of large timescale in lattice–gas automata (LGA) and mesh-free algorithm in molecular dynamics (MD) leading to computational efficiency dramatically higher compared to MD [1]. To fulfill this expectation, the basic component of DPD was defined as a coarse-grained particle which represents a cluster of molecules instead of atoms/molecules themselves. With the larger spatial and time scale, DPD modeling has been successfully used in larger fluid systems which are beyond the capacity of MD simulation; examples include polymer and DNA suspensions [2–4], red blood cells in blood flow [5,6], and platelet aggregation [7].

The interaction between DPD particles consists of the conservative force, the dissipative force and the random force. The conservative force is a soft repulsive force due to the interaction potential between particles. The dissipative force or

* Corresponding author.
E-mail address: george_karniadakis@brown.edu (G.E. Karniadakis).

http://dx.doi.org/10.1016/j.jcp.2014.02.003
0021-9991/

the drag force reduces the velocity difference between particles and hence it dissipates the thermal kinetic energy of the system [8], while the random force generates a stochastic force on each DPD particle. These two forces together satisfy the fluctuation–dissipation theorem and act as a thermostat to maintain the system at a constant temperature [9]. In other words, the DPD method is limited to isothermal systems and is not valid for modeling non-isothermal systems because the total energy of the DPD system is not conserved [10].

To extend the isothermal DPD equations to modeling heat transport in non-isothermal fluid systems, DPD with energy conservation was developed by introducing the internal energy as an additional property to the DPD system [10,11]. The energy-conserving DPD model is known in the literature as eDPD [12]. Similarly to the standard DPD method, each eDPD particle is associated with its internal energy in addition to other quantities such as position and momentum. As a result, the heat transfer can be modeled by the exchange of the internal energy between particles. The eDPD model has been successfully applied to study heat transfer in natural convection [13], heat conduction in nanocomposites [12], heat transfer in nanoparticles suspensions [14] and heat flow [15]. Moreover, with the consideration of energy equation, the eDPD method is able to model phase change [16].

However, the dependence of dynamic properties on temperature has not been correctly modeled in previous eDPD models. In standard DPD and previous eDPD models, the kinematic viscosity of fluid can be roughly predicted [17] by $\upsilon = 45k_BT/4\pi\gamma\rho r_C^3 + 2\pi\gamma\rho r_C^5/1575$ in which the first term is directly proportional to the temperature T, thus the kinematic viscosity increases with increasing temperature; however, the opposite is true. The kinematic viscosity of simple liquids such as water, ethanol and glycerin decreases when the temperature increases [18]. Generally, the diffusivity, viscosity and thermal conductivity of liquids are temperature-dependent and these properties can significantly influence the behavior of viscous flow in non-isothermal systems. It is of importance to model correctly the relationships between the properties of liquid and temperature when non-isothermal fluid systems are considered.

The objective of the present work is to propose a model for capturing the correct temperature-dependent properties of fluids. Specifically, liquid water is used as an example for verifying the eDPD model we propose. The diffusivity and viscosity of liquid water as well as its Schmidt number and Prandtl number in the range of 273 K to 373 K are reproduced with the present eDPD model. The relationships between the dynamic properties of eDPD fluid and the expressions of the dissipative and random forces have been analyzed. The exponent of the weighting function in the dissipative force is chosen as a temperature-dependent variable and, in particular, a simple quadratic function of temperature is suggested. Results for the diffusivity and viscosity as well as Schmidt number at various temperatures are presented and compared with the available experimental data of liquid water. Furthermore, an analytical formula for determining the mesoscopic heat friction is proposed, which is validated by reproducing the experimental data for Prandtl number of liquid water at various temperatures. The proposed method is not limited to liquid water, and it can be readily extended to other fluids for modeling the correct dependence of thermal hydrodynamic properties in terms of temperature.

The paper is organized as follows. In Section 2 we describe details of eDPD formulation and its parameters, including an analytical formula for determining mesoscopic heat friction (Section 2.1) and a methodology for imposing thermal boundary conditions (Section 2.2). Section 3 presents our validation of the eDPD model and the boundary method (Section 3.2), and the performance of the present eDPD model in reproducing correctly the temperature-dependent properties consistent with experiments (Section 3.3). We conclude with a brief summary in Section 4.

2. Governing equations

The energy-conserving dissipative particle dynamics (eDPD) method is developed based on the standard DPD framework [10,11]. Similarly to the standard DPD method, each eDPD particle is considered as a coarse-grained particle, which represents a group of actual fluid molecules instead of atom/molecule directly. The time evolution of an eDPD particle i is governed by the conservation of momentum and energy and is described by the following set of equations [12]:

$$\frac{\mathrm{d}\mathbf{r}_i}{\mathrm{d}t} = \mathbf{v}_i, \tag{1}$$

$$\frac{\mathrm{d}\mathbf{v}_i}{\mathrm{d}t} = \mathbf{F}_i = \sum_{i\neq j}\left(\mathbf{F}_{ij}^C + \mathbf{F}_{ij}^D + \mathbf{F}_{ij}^R\right), \tag{2}$$

$$C_v\frac{\mathrm{d}T_i}{\mathrm{d}t} = q_i = \sum_{i\neq j}\left(q_{ij}^C + q_{ij}^V + q_{ij}^R\right), \tag{3}$$

where t, $\mathbf{r}_i$, $\mathbf{v}_i$ and $\mathbf{F}_i$ denote time, and position, velocity, force vectors, respectively, T_i the temperature, C_v the thermal capacity of eDPD particles and q_i the heat flux between particles. The summation is carried out over all other particles within a cutoff radius r_C. The three components of $\mathbf{F}_i$ including the conservative force $\mathbf{F}_{ij}^C$, dissipative force $\mathbf{F}_{ij}^D$ and random forces $\mathbf{F}_{ij}^R$ are expressed as [17]:

$$\mathbf{F}_{ij}^C = \alpha_{ij}(T)\omega_C(r_{ij})\mathbf{e}_{ij}, \tag{4}$$

$$\mathbf{F}_{ij}^{D} = -\gamma_{ij}\omega_D(r_{ij})(\mathbf{e}_{ij}\cdot\mathbf{v}_{ij})\mathbf{e}_{ij}, \tag{5}$$

$$\mathbf{F}_{ij}^{R} = \sigma_{ij}\omega_R(r_{ij})\xi_{ij}\Delta t^{-1/2}\mathbf{e}_{ij}, \tag{6}$$

where r_{ij} is distance between particles i and j, $\mathbf{e}_{ij}$ the unit vector from particle j to i, and $\mathbf{v}_{ij} = \mathbf{v}_i - \mathbf{v}_j$ the velocity difference. $\omega_C(r)$, $\omega_D(r)$ and $\omega_R(r)$ are the weight functions of $\mathbf{F}^C$, $\mathbf{F}^D$ and $\mathbf{F}^R$, respectively. Here, $\alpha_{ij}(T)$ are repulsive force parameters given by $\alpha_{ij}(T) = 5.0k_BT(\kappa_c^{-1} - 1.0)/\rho$ for recovering the compressibility κ_c of materials of interest [17]; a common choice for liquid water is $\alpha_{ij}(T) = 75.0k_BT/\rho$ in which k_B is the Boltzmann constant, T the temperature and ρ the number density of the eDPD particles. Also, γ_{ij} are the dissipative coefficients and σ_{ij} are the strengths of random force. ξ_{ij} are symmetric Gaussian random variables with zero mean and unit variance, and are independent for different pairs of particles and at different times [19]. The dissipative force and random force together act as a thermostat when the dissipative coefficient γ_{ij} and the amplitudes of white noise σ_{ij} satisfy the fluctuation–dissipation theorem [10] requiring $\sigma_{ij}^2 = 4\gamma k_BT_iT_j/(T_i + T_j)$ and $\omega_D(r) = \omega_R^2(r)$. A common choice of the weight function is $\omega_C(r) = 1 - r/r_C$ and $\omega_D(r) = \omega_R^2(r) = (1 - r/r_C)^s$ for $r \leqslant r_C$ and zero for $r > r_C$.

The heat flux between particles accounting for the collisional heat flux q^C, viscous heat flux q^V, and random heat flux q^R are given by [12,13,20]:

$$q_i^C = \sum_{j\neq i} k_{ij}\omega_{CT}(r_{ij})\left(\frac{1}{T_i} - \frac{1}{T_j}\right), \tag{7}$$

$$q_i^V = \frac{1}{2C_v}\sum_{j\neq i}\left\{\omega_D(r_{ij})\left[\gamma_{ij}(\mathbf{e}_{ij}\cdot\mathbf{v}_{ij})^2 - \frac{(\sigma_{ij})^2}{m}\right] - \sigma_{ij}\omega_R(r_{ij})(\mathbf{e}_{ij}\cdot\mathbf{v}_{ij})\zeta_{ij}\right\}, \tag{8}$$

$$q_i^R = \sum_{j\neq i}\beta_{ij}\omega_{RT}(r_{ij})dt^{-1/2}\zeta_{ij}^e, \tag{9}$$

where k_{ij} and β_{ij} determine the strength of the collisional and random heat fluxes. The parameter k_{ij} plays the role of a thermal conductivity given as $k_{ij} = C_v^2\kappa(T_i + T_j)^2/4k_B$ in which κ is interpreted as mesoscale heat friction coefficient [11–14], and $\beta_{ij}^2 = 2k_Bk_{ij}$. The weight functions $\omega_{CT}(r)$ and $\omega_{RT}(r)$ in Eqs. (7) and (9) are given as $\omega_{CT}(r) = \omega_{RT}^2(r) = (1 - r/r_C)^{s_T}$ in which s_T is the exponent of the weight functions. The case of $s_T = 2.0$ corresponds to the typical quadratic weighting function, which is adopted in the present work following the choice of Refs. [14,20,21].

Dimensionless variables that are suitable for interpretation of the results are introduced to carry out the simulations. The temperature of reference $T^* = 300$ K is used to scale the temperatures, thus the temperatures ranging from 273 K to 373 K are represented by the dimensionless temperature $T = 0.91$ to 1.2433. The heat capacity of each eDPD particle is normalized by the Boltzmann constant k_B^* given by $C_v = C_v^*L^{*3}/\rho k_B^*$ in which C_v^* is the volumetric heat capacity of the fluid, L^* the length of reference, and ρ the number density of eDPD particles. For example, $C_v^* = 4.167\times10^6$ J m^{-3} K^{-1} for water at 300 K and $k_B^* = 1.381\times10^{-23}$ J K^{-1}, so given a length unit $L^* = 11$ nm and $\rho = 4.0$ one gets $C_v = 1.0\times10^5$ for the simulations. All the quantities without physical units are the dimensionless variables from now on.

2.1. Mesoscale heat friction

The transport properties including diffusivity, viscosity and thermal diffusivity of the eDPD fluid are output properties instead of input parameters. Several researchers [2,17,22] have investigated the expression of the diffusivity and the viscosity in terms of DPD parameters. With the interaction between particles described by Eqs. (4)–(6) and $\omega_D(r) = \omega_R^2(r) = (1 - r/r_C)^s$, a rough prediction of diffusivity and kinematic viscosity can be obtained by assuming the radial pair distribution function $g(r) = 1.0$ corresponding to ideal gases [2,17]. This assumption simplifies the derivations and as reported in Ref. [17] it leads to approximately 10–30% deviation from the computed results. The weighting function versus r/r_C for various exponents is plotted in Fig. 1. It clearly shows that smaller s yields a stronger particle interaction than the standard quadratic one for a given configuration of particles. Thus, the variation of the exponent s results in the changes of the diffusivity and the viscosity. Similar to the method mentioned in Refs. [2,17] the diffusivity of the eDPD fluid can be approximated by:

$$D = \frac{3k_BT(s+1)(s+2)(s+3)}{8\pi\gamma\rho r_C^3}. \tag{10}$$

The kinematic viscosity of a simple DPD system consists of two parts and can be approximated by:

$$\upsilon = \frac{3k_BT(s+1)(s+2)(s+3)}{16\pi\gamma\rho r_C^3} + \frac{16\pi\gamma\rho r_C^5}{5(s+1)(s+2)(s+3)(s+4)(s+5)}, \tag{11}$$

where the first term is the contribution from the diffusion motion of particles while the second term is from the dissipative forces. The standard DPD model is only valid for isothermal systems, since the fluctuation–dissipation theorem yields the

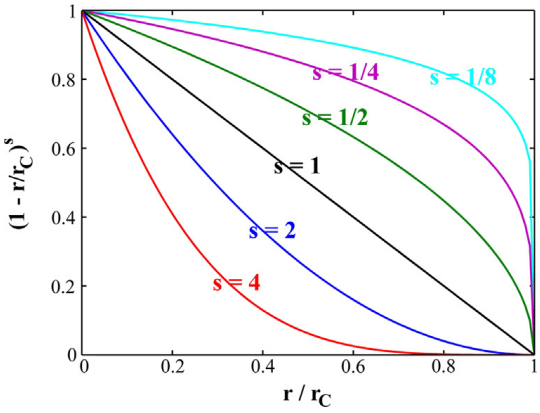

Fig. 1. Generalized weighting functions of the dissipative force and the random force for different exponent s.

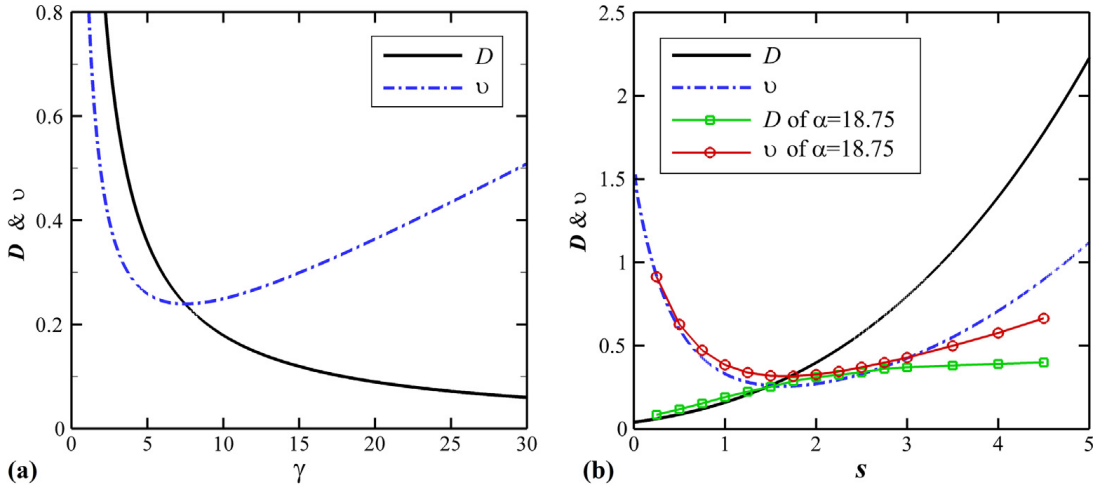

Fig. 2. (a) Effect of the dissipative coefficient γ on the diffusivity D and the kinematic viscosity υ of eDPD fluid calculated by Eqs. (10) and (11). (b) Effect of the exponent s of the weighting function on the diffusivity D and the kinematic viscosity υ of eDPD fluid. The solid and dashed lines are the values of D and υ calculated by Eqs. (10) and (11) while the lines with symbols are the values of D and υ obtained by individual eDPD simulations at $\rho = 4.0$, $\alpha = 18.75 k_B T$, $\gamma = 4.5$, $r_C = 1.0$ and $k_B T = 1.0$.

relationship $\sigma^2 = 2\gamma k_B T$; taking σ or γ as a constant makes no difference to the DPD system. However, for non-isothermal systems, the thermal fluctuation becomes larger as the temperature increases. Keeping σ constant means that the strength of thermal fluctuation does not change with the variation of temperature, which is contrary to the physics. We use γ rather than σ in Eqs. (10) and (11) because given γ the strength of random force $\sigma = \sqrt{2\gamma k_B T}$ increases with the increase of temperature, which is consistent with the physics.

Eqs. (10) and (11) indicate that both the diffusivity D and the kinematic viscosity υ of the eDPD fluid increase with the increase of temperature when the variables in Eqs. (10) and (11) (except temperature) are kept constant. However, for most of the simple liquids such as water, ethanol and glycerin, the diffusivity increases but the kinematic viscosity decreases with increasing temperature [18]. In order to simulate the flow dynamics of such liquids, at least one of the parameters ρ, r_C, γ and s should be function of temperature so that the eDPD model can reproduce the correct dynamic behavior of non-isothermal fluid systems. The number density ρ and the cutoff radius r_C are fixed after the fluid system is constructed, and they are not variables in the eDPD system. Thus, only the dissipative coefficient γ and the exponent of the weighting function s can be modeled as functions of temperature.

Fig. 2(a) illustrates the effect of the dissipative coefficient γ on the diffusivity D and the kinematic viscosity υ of an eDPD fluid. To obtain smaller viscosity and larger diffusivity, one has to reduce the value of γ when the temperature increases, since the amplitude of the Gaussian white noise is related to γ and given by $\sigma^2 = 2\gamma k_B T$, the reduction of the dissipative coefficient γ means that hotter systems have smaller thermal fluctuations, which is contrary to the correct physics. Thus, the dissipative coefficient γ cannot be defined as such a function of temperature for modeling the temperature-dependent diffusivity and viscosity of eDPD fluid. Fig. 2(b) shows the effect of the exponent of the weighting function s on the diffusivity D and the kinematic viscosity υ of eDPD fluid. For most of the simple liquids, their diffusivity increases but the kinematic viscosity decreases when the temperature increases. It can be found in Fig. 2(b) that D increases while υ decreases with increasing s when $0 < s < 1.5$.

However, Eqs. (10) and (11) are obtained in the context of zero conservative force and can give only a rough estimate of the diffusivity and the viscosity of eDPD systems [17]. In practice, eDPD simulations include the conservative force which

would affect the properties of eDPD fluid. To verify that the range of $0 < s < 1.5$ is still valid in the presence of conservative force, individual eDPD simulations with repulsive coefficient $\alpha = 75k_BT/\rho$ are carried out to study the effect of s on the diffusivity and the viscosity. Results in Fig. 2(b) show that Eqs. (10) and (11) for estimating the values of D and υ are quite accurate in the range of $0 < s < 1.5$. Furthermore, Fig. 2(b) reveals that the range of 0 to 1.5 is still valid for modeling the temperature-dependent properties after the conservative force is included.

Suppose s is a function of temperature and the dissipative coefficient γ is a constant, the amplitude of the Gaussian white noise given by $\sigma^2 = 2\gamma k_B T$ would increase as temperature increases, which indicates that hotter systems have larger thermal fluctuations consistent with the physical intuition. Thus, the exponent of the weighting function s is a good option for modeling the temperature-dependent diffusivity and viscosity of eDPD fluids. In the present work, s is defined as a function of instantaneous temperature of the eDPD particles, and the details for choosing the function for s will be introduced in Section 3.3.

Similar to the diffusivity and the kinematic viscosity, the thermal conductivity is an output property as well. It is necessary to construct the relationship between the macroscopic thermal conductivity and eDPD parameters. Considering an eDPD system whose transport of energy is dominated by the dissipative interactions, the macroscopic thermal conductivity η can be calculated by [15,23]:

$$\eta = \frac{2\pi}{3}\frac{\rho^2}{T^2}\int_0^{r_C} r^4 k\omega_{CT}(r)g(r)\,dr, \tag{12}$$

where $k = C_v^2\kappa T^2/k_B$ and $\omega_{CT}(r)$ the weight function used in Eq. (7). Given $\omega_{CT}(r) = (1 - r/r_C)^{s_T}$ an analytical prediction for the thermal conductivity η can be obtained by assuming the radial pair distribution function $g(r) = 1.0$ corresponding to ideal gases, and it is given as:

$$\eta = \frac{16\pi\rho^2\kappa C_v^2 r_C^5}{k_B(s_T+1)(s_T+2)(s_T+3)(s_T+4)(s_T+5)}. \tag{13}$$

Specifically, when the typical quadratic weighting function $(1-r/r_C)^2$ is employed for $\omega_{CT}(r)$ with $s_T = 2.0$, then Eq. (13) becomes

$$\eta = \frac{2\pi\rho^2}{315k_B}\kappa C_v^2 r_C^5. \tag{14}$$

The definition of the Prandtl number is $Pr = \rho\upsilon C_v/\eta$, which is a temperature-dependent dimensionless number and its value can be obtained from available experimental data [18]. After replacing η by Pr in Eq. (14), we have a formula for determining the mesoscale heat friction κ for the eDPD system given by:

$$\kappa = \frac{315k_B\upsilon}{2\pi\rho C_v r_C^5}\frac{1}{Pr}, \tag{15}$$

where υ is the kinematic viscosity which can be roughly approximated by Eq. (11) or given by the computed kinematic viscosity. The expression of Eq. (15) is obtained based on the typical quadratic weighting function $\omega_{CT}(r) = (1 - r/r_C)^2$ and a similar formula can be derived from Eq. (12) when a different weighting function is employed.

2.2. Boundary conditions

The boundary conditions at the mesoscale are crucial for the investigation of heat transfer in non-periodic systems. Freezing some particles at desired boundaries but allowing them to interact with fluid particles is a common treatment in DPD for modeling the surface of solid objects [24,25]. Since these solid walls made up by discrete particles induce large unwanted density fluctuations in the vicinity of the walls [19], many attempts [19,24–26] have been made to reduce the density fluctuations. Alternatively, Lei et al. [27] used effective forces to represent the presence of solid wall boundaries. In the present work, we extend this boundary method to non-isothermal DPD systems for applying thermal boundary conditions. Both the force and the heat flux contributions from the boundaries are imposed onto the particles for which the distance from the boundaries is less than the cutoff radius r_C. Since the solid wall particles are replaced by effective forces and heat fluxes, there is no wall particles in the simulations when the boundary method is employed.

The effective boundary force and heat flux are extracted from the fluid–solid interactions using the continuum approximation. We integrate the force and heat flux contributions weighted by the local structure of the fluid which is described by the radial distribution function $g(r)$ over the part of the cutoff sphere that lies outside of the fluid domain, as shown with the dark volume of Fig. 3. We choose a coordinate system with x-axis along the direction of the velocity component of particle i parallel to the wall surface and z-axis perpendicular to the wall surface. $\Delta\mathbf{V} = \mathbf{v}_i - \mathbf{U}$ is the instantaneous velocity difference between particle i with velocity $\mathbf{v}_i$ and the wall boundary with velocity $\mathbf{U}$, while u and w denote the x and z components of $\Delta\mathbf{V}$, respectively.

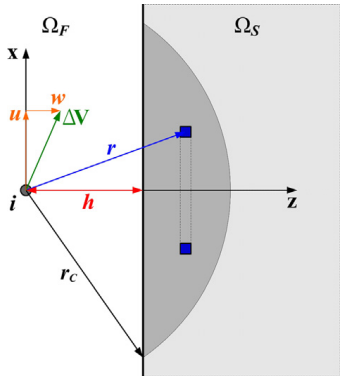

Fig. 3. Integration domains for the effective boundary force and heat flux. Ω_F and Ω_S represent the domain of fluid and solid wall, respectively. The number of particles in the infinitesimal ring element is $2\pi\rho g(r)x\,dx\,dz$ in which ρ is the average number density and $g(r)$ the radial distribution function. ΔV is the instantaneous velocity difference between particle i and the wall boundary.

Consider a planar wall surface or a wall surface with the radius of curvature far greater than the cutoff radius r_C, then the total conservative force $\mathbf{F}_C(h)$ on the particle i due to the presence of wall boundary can be evaluated by:

$$\mathbf{F}_C(h) = 2\pi\rho\mathbf{n}_w \int_{z=h}^{r_C} \int_{x=0}^{\sqrt{r_C{}^2-z^2}} F^C(r)g(r)\frac{z}{r}x\cdot dx\cdot dz = f^C(h)\mathbf{n}_w, \tag{16}$$

where $\mathbf{n}_w$ is the normal unit vector of the wall surface, ρ the number density of the eDPD particles, h the distance between the particle and the wall boundary, and $r=\sqrt{x^2+z^2}$ as shown in Fig. 3. The x and y components of $\mathbf{F}_C(h)$ parallel to the wall surface vanish due to spherical symmetry. The value of the effective conservative force $f^C(h)$ is interpreted as the pressure force in Ref. [28] to eliminate density fluctuations in the vicinity of the wall boundary.

The x component of the effective dissipative force on the particle i contributed by the wall boundary can be calculated by:

$$\begin{aligned}\mathbf{F}_{D\parallel}(h) &= -\pi\rho\gamma u\mathbf{e}_x \int_{z=h}^{r_C} \int_{x=0}^{\sqrt{r_C{}^2-z^2}} \omega_D(r)g(r)x^3\cdot dx\cdot dz \\ &= -\gamma_{D\parallel}(h)u\mathbf{e}_x,\end{aligned} \tag{17}$$

where $\gamma_{D\parallel}(h)$ is a function of distance from the particle i to the wall surface and $\mathbf{e}_x$ the unit vector of x-axis.

Remark 1. The expression of $\mathbf{F}_{D\parallel}(h)$ is different from the formula in Ref. [27] because the authors used the assumption of linear velocity profile in the boundary, but our wall boundary is considered as a rigid body and has uniform velocity $\mathbf{U}$.

The z component of the effective dissipative force on particle i is calculated by:

$$\begin{aligned}\mathbf{F}_{D\perp}(h) &= -2\pi\rho\gamma w\mathbf{e}_z \int_{z=h}^{r_C} \int_{x=0}^{\sqrt{r_C{}^2-z^2}} \omega_D(r)g(r)xz^2\cdot dx\cdot dz \\ &= -\gamma_{D\perp}(h)w\mathbf{e}_z.\end{aligned} \tag{18}$$

Then, the total dissipative force on particle i due to the presence of wall boundary is

$$\mathbf{F}_D(h) = -\gamma_{D\parallel}(h)u\mathbf{e}_x - \gamma_{D\perp}(h)w\mathbf{e}_z, \tag{19}$$

where the negative signs indicate the x and z components of the effective dissipative force are in the opposite directions of the relative velocity vectors $u\mathbf{e}_x$ and $w\mathbf{e}_z$. In addition, the effective random force representing the fluctuation part of interactions with the wall particles is given by [27]:

$$\mathbf{F}_R(h) = \left(\sigma_{R\parallel}(h)\mathbf{e}_x + \sigma_{R\perp}(h)\mathbf{e}_z\right)\xi, \tag{20}$$

where ξ is the random variable with Gaussian distribution, $\sigma^2_{R\parallel}(h) = 2k_BT\gamma_{D\parallel}(h)$ and $\sigma^2_{R\perp}(h) = 2k_BT\gamma_{D\perp}(h)$.

For an isothermal wall, the temperature of the wall is fixed, and let us denote it by T_w; similarly to the calculation of the forces in Eqs. (16)–(20), we have the effective collisional heat flux due to the presence of the wall boundary:

$$q_C(h) = 2\pi\rho \int_{z=h}^{r_C} \int_{x=0}^{\sqrt{r_C^2-z^2}} q^C(r) g(r) x \cdot dx \cdot dz$$
$$= \frac{\pi\rho C_v^2 \kappa}{2k_B} \int_{z=h}^{r_C} \int_{x=0}^{\sqrt{r_C^2-z^2}} \omega_{CT}(r) g(r) x \cdot dx \cdot dz \cdot (T_i + T_w)^2 \left(\frac{1}{T_i} - \frac{1}{T_w}\right)$$
$$= \phi(h) \cdot (T_i + T_w)^2 \left(\frac{1}{T_i} - \frac{1}{T_w}\right), \tag{21}$$

where T_i is temperature of particle i and $\phi(h)$ is a function of the height from the particle i to the wall surface. Eq. (21) reveals that the effective collisional heat flux is affected by the difference of temperature between the particle i and the wall boundary as well as their distance. The viscous component of the effective heat flux can be evaluated by:

$$q_V(h) = \frac{\pi\rho}{2C_v} \int_{z=h}^{r_C} \int_{x=0}^{\sqrt{r_C^2-z^2}} \omega_D(r)\left(\gamma u^2 x^2 + 2\gamma w^2 z^2 - 2\sigma^2\right) g(r) x \cdot dx \cdot dz, \tag{22}$$

where u and w denote the x and z components of the velocity difference $\Delta\mathbf{V} = \mathbf{v}_i - \mathbf{U}$ shown in Fig. 3. The third term of Eq. (8) induced by the random force has zero mean thus it is ignored in the integration. The random component of the effective heat flux is given as:

$$q_R(h) = \varphi(h) \cdot \xi^e, \tag{23}$$

where ξ^e is an independent identically distributed random variable with Gaussian distribution independent of ξ, and $\varphi^2(h) = 2k_B(T_i + T_w)^2\phi(h)$ is obtained from the relationships of $\omega_{RT}^2(r) = \omega_{CT}(r)$ and $\beta_{ij}^2 = 2k_B k_{ij}$ where $k_{ij} = C_v^2\kappa(T_i + T_j)^2/4k_B$ in Eqs. (7) and (9).

Remark 2. For non-isothermal systems the radial distribution function $g(r)$ is calculated as follows in order to take into account of its temperature dependence. When different temperatures T and the number densities ρ are expected on the wall boundaries, their $g(r)$ should be calculated independently. In practice, we estimate the number density ρ and the temperature T on the wall boundaries and construct small periodic systems with these ρ and T for obtaining their $g(r)$. With estimated $g(r)$ and ρ the effective forces and heat fluxes can be computed by Eqs. (16)–(23). If the effective forces and heat fluxes induce significant density or temperature fluctuations, according to the results based on these effective forces and heat flues, corresponding corrections on the estimate of ρ and T are made until no significant fluctuation is observed in the vicinity of wall boundaries.

3. Results

3.1. Verification of energy conservation

The eDPD framework is supposed to be energy conserving [10]. However, to the best of our knowledge, no eDPD simulation has been carried out to verify the energy conservation of the system. To check if the eDPD system has total energy drift an eDPD simulation in a periodic domain of size $20.0 \times 20.0 \times 20.0$ containing 32 000 eDPD fluid particles is performed. The total energy E of an eDPD system consists of the potential energy $P_E = \sum -\frac{1}{2}\alpha r_C(1 - r/r_C)^2$, the kinetic energy $K_E = \sum \frac{1}{2}mV^2$ and the internal energy $I_E = \sum C_v(T - T_0)$ in which T is the temperature of eDPD particles and T_0 is a reference temperature. The simulations are performed with the open source code LAMMPS [29], and a modified velocity-Verlet algorithm [17] is utilized for the numerical integration of the eDPD equations with time step $dt = 0.005, 0.01$ and 0.02. We plot the history of energies of the eDPD system during the simulation, as shown in Fig. 4. Results show that the eDPD model does conserve the total energy of the system. The fluctuation of the total energy E is less than 0.1% and there is almost no difference between the results of $dt = 0.005$ and $dt = 0.01$. However, compared to the results of $dt = 0.005$ and $dt = 0.01$, a larger time step $dt = 0.02$ induces a slight drift in the potential energy P_E and the total energy E. This reveals that the error is induced by time integration, which can be eliminated by using smaller time steps or a better time integration scheme.

3.2. Validation of Fourier law

To validate the present eDPD formulation and the proposed boundary method, we simulate Poiseuille flow with a simple eDPD fluid. First, a simulation of an equilibrium system of $20.0 \times 20.0 \times 20.0$ in DPD units with periodic boundary condition in three directions was carried out for obtaining the radial distribution function $g(r)$ of the eDPD particles, which is

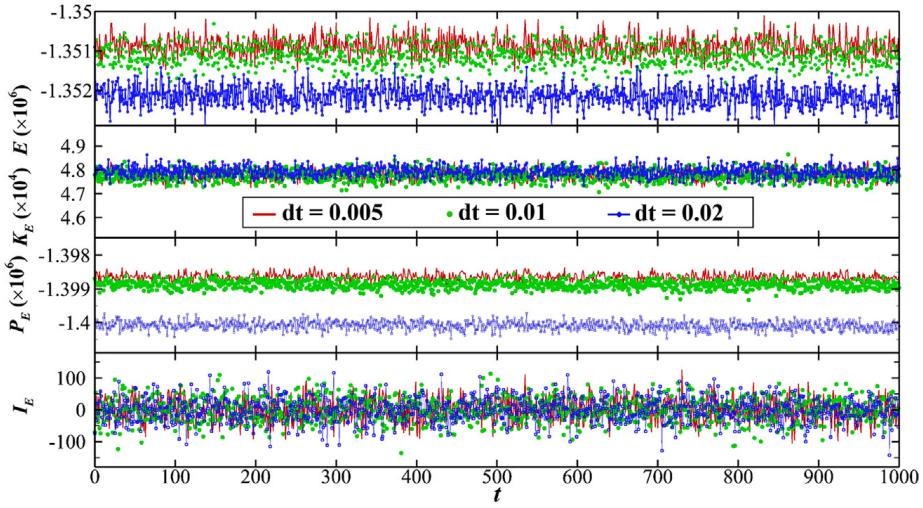

Fig. 4. History of the total energy E (top), the kinetic energy K_E (second from top), the potential energy P_E (second from bottom) and the internal energy I_E (bottom) of an eDPD system during simulations with three time steps $dt = 0.005, 0.01$ and 0.02. The results are based on the set of parameters $\rho = 4.0$, $k_BT = 1.0$, $\alpha = 18.75k_BT$, $\gamma = 4.5$, $r_C = 1.58$, $s = 0.41 + 1.9(T^2 - 1)$, $C_v = 1.0 \times 10^5$ and κ is given by Eq. (15).

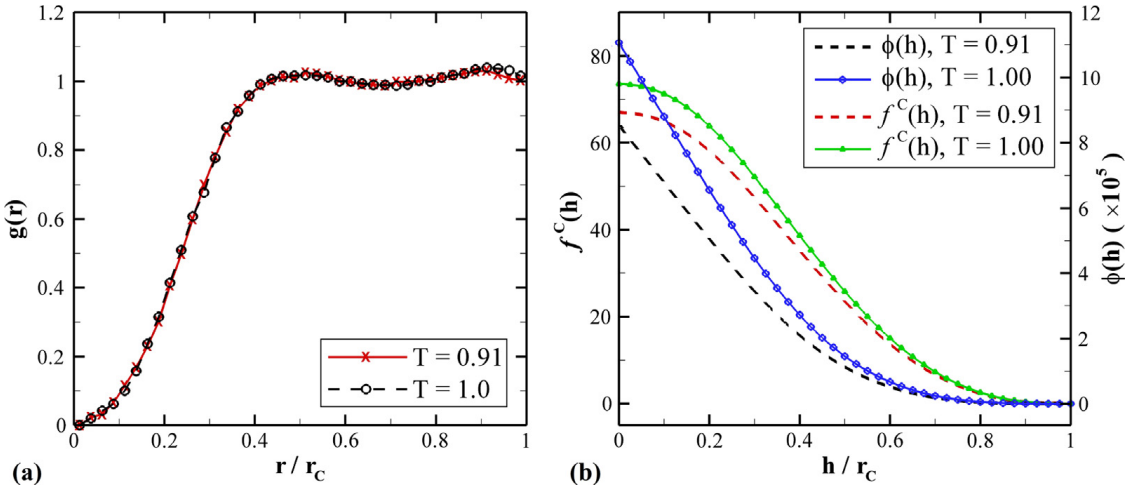

Fig. 5. (a) Radial distribution function $g(r)$ of the eDPD particles. (b) $f^C(h)$ calculated by the integration in Eq. (16) and $\phi(h)$ calculated by the integration in Eq. (21). The curves are based on the parameters of $\rho = 4.0$, $\alpha = 18.75k_BT$, $\gamma = 4.5$, $r_C = 1.58$, $s = 0.41 + 1.9(T^2 - 1)$, $C_v = 1.0 \times 10^5$ and κ is given by Eq. (15).

necessary for computing the effective boundary forces and heat fluxes by Eqs. (16)–(23) representing the solid walls at the upper and lower boundaries.

Fig. 5(a) shows the radial distribution function $g(r)$ of the eDPD particles; it has a slight difference when T is changed from 0.91 to 1.00. All the three components of the effective boundary force as well as the effective boundary heat flux can be obtained by Eqs. (16)–(23) using the computed $g(r)$ shown in Fig. 5(a). The conservative component of the boundary force $f_C(h)$ and the collisional component of boundary heat flux are plotted in Fig. 5(b). The curves in Fig. 5(b) clearly show that both $f_C(h)$ and $\phi(h)$ are decreasing functions of h. The value of $f_C(h)$ for $T = 1.00$ is greater than that for $T = 0.91$ because the repulsive parameter α_{ij} of the conservative force $\mathbf{F}_{ij}^C$ varies directly with the temperature T. Other components of the effective forces and heat fluxes have similar curves. Then, the best fitting functions of these curves are utilized to impose the effective boundary force and effective boundary heat flux on the eDPD particles whose distance from wall boundaries is less than the cutoff radius r_C.

For the Poiseuille flow with pressure gradient acting in the x-direction on a fluid between two plates in the xy-plane, both the velocity component and the pressure gradient in the vertical z-direction vanish identically so that the x-component of the velocity u is dependent on only z and time t. In this simple case, the Navier–Stokes equations admit the exact time-dependent solution given by [28]:

$$u(z,t) = \frac{Fd^2}{8\upsilon}\left(1 - \left(\frac{2z}{d}\right)^2\right) - \sum_{n=0}^{\infty} \frac{4(-1)^n Fd^2}{\upsilon\pi^3(2n+1)^3} \cdot \cos\left[\frac{(2n+1)\pi z}{d}\right] \cdot \exp\left[-\frac{(2n+1)^2\pi^2\upsilon t}{d^2}\right], \tag{24}$$

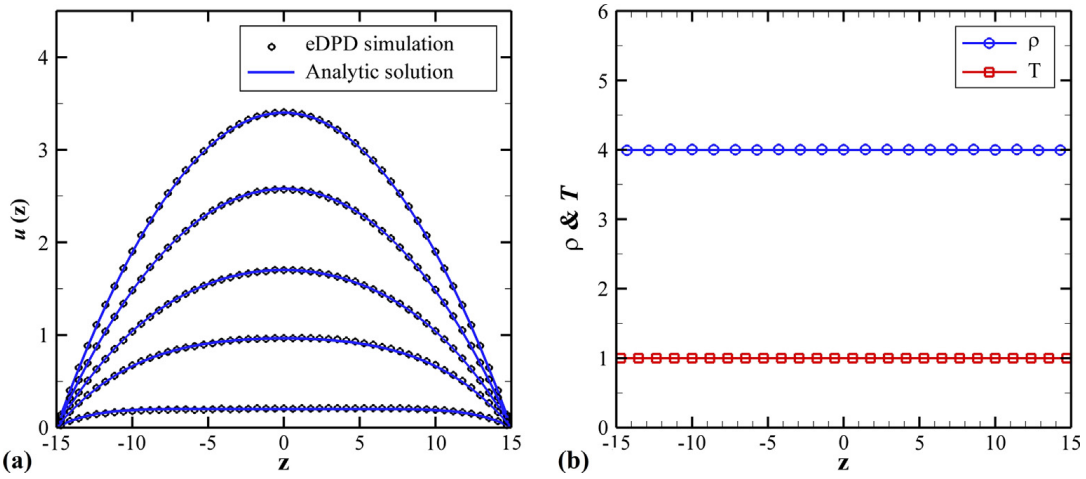

Fig. 6. (a) Time-evolution of the velocity profile in Poiseuille flow and comparison with theoretical predictions at $t = 1.0$, 5.0, 10.0, 20.0 and at steady state. (b) Density ρ, and temperature T profiles in Poiseuille flow with $\rho = 4.0$, $\alpha = 18.75$, $\gamma = 4.5$, $r_C = 1.58$, $s = 0.41$ and the computed kinematic viscosity of eDPD fluid is 6.62. The simulation uses 43 200 particles in an isothermal computational domain of $60.0 \times 6.0 \times 30.0$ in DPD units at $k_B T = 1.0$.

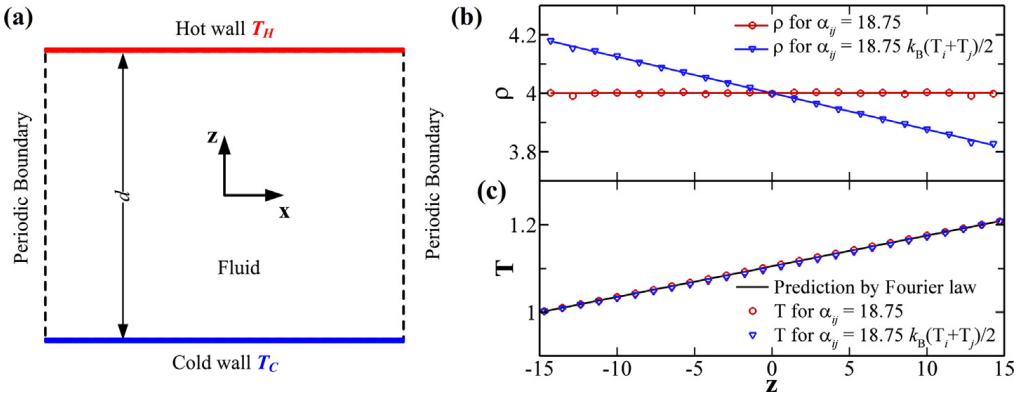

Fig. 7. (a) Schematic of the geometry for the steady-state heat conduction between a cold wall T_C and a hot wall T_H. (b) Density ρ and (c) temperature T profiles in the heat conduction between a cold wall ($T_C = 1.0$) at $z = -15.0$ and a hot wall ($T_H = 1.21$) at $z = 15.0$. The simulations use 43 200 eDPD particles in a computational domain $60.0 \times 6.0 \times 30.0$ in DPD units. The circle symbols represent the numerical results with constant α_{ij} while gradient symbols for $\alpha_{ij} = 18.75 k_B (T_i + T_j)/2$.

where d is the separation of the plates, υ the kinematic viscosity, and F a force per unit mass given by:

$$F = \frac{1}{\rho}\frac{\partial p}{\partial x} = g_x, \tag{25}$$

where $\partial p/\partial x$ is the pressure gradient. A body force field g_x is applied on each eDPD particle, which is equivalent to imposing a pressure drop of $\rho g L_x$ on the channel of length L_x. The eDPD parameters for the Poiseuille flow are listed in the caption of Fig. 6. The computational domain is divided into 51 bins along the z-direction. All local flow properties are obtained by averaging enough sampled data. The transient velocity profiles are collected by carrying out 100 simulations from different random seeds. The development of velocity profiles is shown in Fig. 6(a), as well as the density and temperature profile in Fig. 6(b). The velocity profiles are in an excellent agreement with the theoretical solution given by Eq. (24). We also found that density and temperature fluctuations near the boundaries are negligible.

The next test case for validation is heat conduction between a cold wall and a hot wall. Fig. 7(a) illustrates the geometry of the problem, with the stationary fluid confined between a hot wall of $T_H = 1.21$ and a cold wall of $T_C = 1.00$. The Fourier law gives linear spatial distribution of temperature for the steady-state heat conduction. Similarly to the last case, independent simulations of an equilibrium system at $k_B T = 1.21$ and 1.00 are carried out for obtaining the radial distribution function $g(r)$ of eDPD particles. Then the effective boundary forces and heat fluxes are calculated for imposing the desired boundary condition on the fluid system. First, we use a constant conservative coefficient α_{ij}, which does not consider the variation of density when the temperature changes. Then a temperature-dependent conservative coefficient given by $\alpha_{ij} = 75 k_B T/\rho$ is used [17] to consider the effect of temperature on the density of fluid. Fig. 7(c) shows that both expressions of α_{ij} lead to the correct behavior of heat conduction in agreement with Fourier law. However, the profiles of the density are different: constant α_{ij} leads to a uniform density distribution, but temperature-dependent α_{ij} results in lower density for the hot fluid and higher density for the cold fluid as shown in Fig. 7(b), which is qualitatively consistent with the character of simple fluids such as water. The fluid density of the case $\alpha_{ij} = 18.75 k_B T$ is linear to temperature

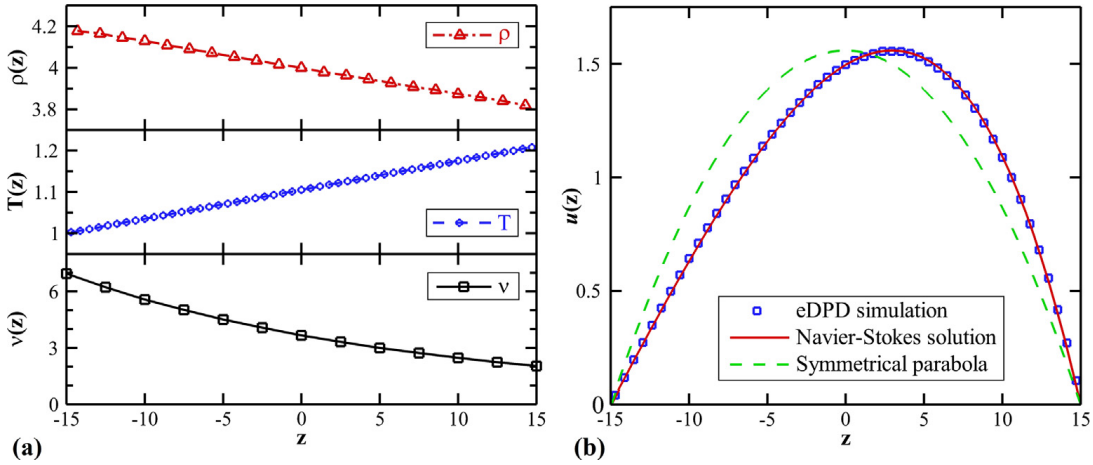

Fig. 8. Poiseuille flow combined with the heat conduction between a cold wall T_C and a hot wall T_H. (a) Density ρ, temperature T and viscosity ν profiles between the cold wall ($T_C = 1.0$) at $z = -15.0$ and the hot wall ($T_H = 1.21$) at $z = 15.0$. (b) Velocity profile in the Poiseuille flow with heat conduction and comparison with Navier–Stokes solution based on variable viscosities along the z direction. The simulations use 43,200 eDPD particles in a computational domain $60.0 \times 6.0 \times 30.0$ in DPD units. The circle symbols represent the numerical results with constant α_{ij} while gradient symbols for $\alpha_{ij} = 18.75 k_B (T_i + T_j)/2$.

because a simple linear function is used for α_{ij}. The results in Fig. 7(b) reveal that the effect of the temperature on the fluid density can be modeled in eDPD by applying a temperature-dependent conservative force between eDPD particles.

We have validated the non-isothermal model for hydrodynamic flow and heat conduction separately. It is necessary to carry out one more test case including both hydrodynamic flow and heat conduction. A body force g_x is applied on the fluid confined between a hot wall of $T_H = 1.21$ and a cold wall of $T_C = 1.00$. Since the viscosity of hotter fluid is smaller than that of colder fluid, as shown in Fig. 8(a), the variation of the viscosity along the z direction leads to an asymmetric velocity profile. Fig. 8(b) shows the velocity profile; the peak of the velocity profile shifts to the side corresponding to the hotter fluid. Given the viscosity profile $\upsilon(z)$ shown in Fig. 8(a), we numerically solve the Navier–Stokes equation $\nabla(\upsilon(z) \cdot \nabla \mathbf{V}) = g_x$ and obtain the velocity profile. The results show that the eDPD simulation gives a velocity profile in agreement with the continuum Navier–Stokes solution and the no-slip boundary condition is expected when the boundary method is employed.

3.3. Temperature-dependent properties

The above three cases validate both the eDPD formulation and the boundary method. For an isothermal fluid system, the present model captures the correct behavior of fluid as the standard DPD does. For a non-isothermal fluid system, the present model can reproduce Fourier law in heat conduction between a hot wall and a cold wall. Our next objective is to construct a model for capturing the correct dynamic properties of common fluids in non-isothermal systems.

The liquid water is employed as an example fluid in the present study; the experimental data of its self-diffusivity at various temperature is taken from Ref. [30] and the kinematic viscosity is taken from Ref. [18]. At $T^* = 300$ K the diffusivity of liquid water is 2.41×10^{-9} m^2 s^{-1} and the kinematic viscosity is 8.57×10^{-7} m^2 s^{-1} hence the Schmidt number $\mathrm{Sc} = \upsilon/D = 355.60$. To capture the correct Schmidt number at $T = 1.0$ the parameters in eDPD system are defined as $\rho = 4.0$, $\alpha_{ij} = 75 k_B T/\rho$, $\gamma = 4.5$, $\sigma^2 = 2 k_B T \gamma$, $r_C = 1.58$ and $s_0 = 0.41$. From the eDPD simulations, we know that the viscosity is affected strongly by the value of s as it changes the envelope of interaction. Considering the effect of temperature on the dynamic properties of eDPD fluid, s is defined as a function of the temperature to reproduce the experimental data of materials of interest. In the present work, a simple expression $s(T) = C_1 + C_2(T^2 - 1)$ is used and the coefficients C_1 and C_2 are optimized to get consistent transport properties with the experimental data of liquid water. In the simulations we use $s = 0.41 + 1.9(T^2 - 1)$ so that $0 < s < 1.5$ when the dimensionless temperature T changes between 0.91 and 1.2433.

As mentioned in Section 2.1 the diffusivity, kinematic viscosity and thermal conductivity are output properties instead of input parameters. Although they can be roughly predicted by Eqs. (10), (11) and (13), respectively, their exact values can be only obtained by simulating the eDPD system. We determine the self-diffusivity of the eDPD system by the mean-square displacement

$$D = \lim_{t \to \infty} \frac{1}{6t} \left\langle \left| \mathbf{r}(t) - \mathbf{r}(0) \right|^2 \right\rangle, \tag{26}$$

where $|\mathbf{r}(t) - \mathbf{r}(0)|^2$ is the mean-square displacement (MSD). Fig. 9(a) shows the MSD of the eDPD system at $T = 0.91$, 1.00 and 1.11. The MSD has been scaled by 6.0 thus the slope of the line is the self-diffusivity for each case. It can be found in Fig. 9(a) that the diffusivity increases when the temperature increases.

The kinematic viscosity of the eDPD system is computed from the periodic Poiseuille flow method [31]. The velocity profile obtained for the periodic Poiseuille flow is shown in Fig. 9(b). The kinematic viscosity can be determined by fitting the velocity profile with the analytical solution $u(z) = g_x z(d - |z|)/2\upsilon$ in which υ is the kinematic viscosity, $g_x = 0.20$ the

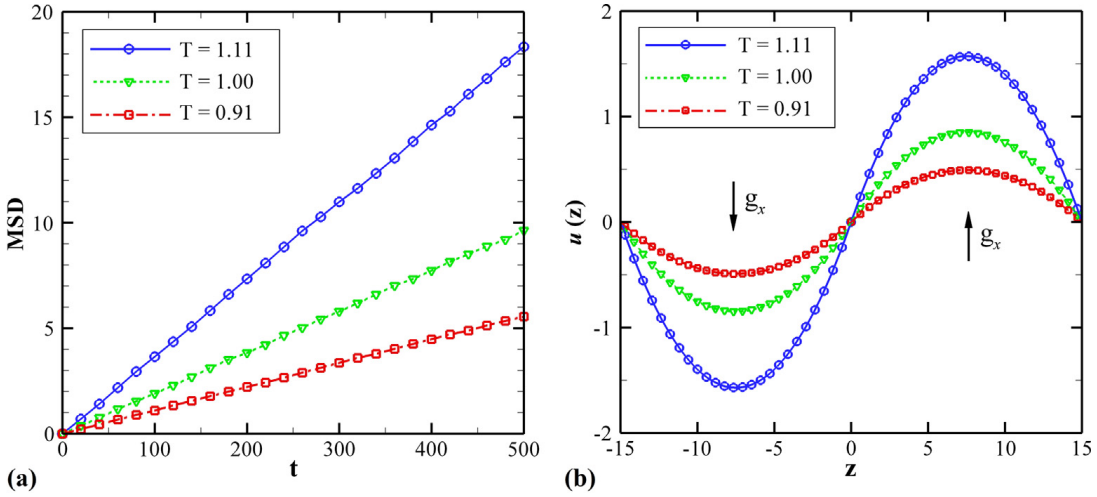

Fig. 9. (a) Mean-square displacement (scaled by 6.0) of eDPD particles for different temperatures. The slopes of the lines are the self-diffusivity of eDPD fluid. (b) Velocity profiles obtained using the periodic Poiseuille flow method for different temperatures. The lines are quadratic fitting curves for each case. The simulations are carried out in a computational domain of $30.0 \times 6.0 \times 30.0$ in DPD units with $\rho = 4.0$, $\alpha_{ij} = 18.75 k_B (T_i + T_j)/2$, $\gamma = 4.5$, $r_C = 1.58$, $s = 0.41 + 1.9(T^2 - 1)$ and $g_x = 0.2$.

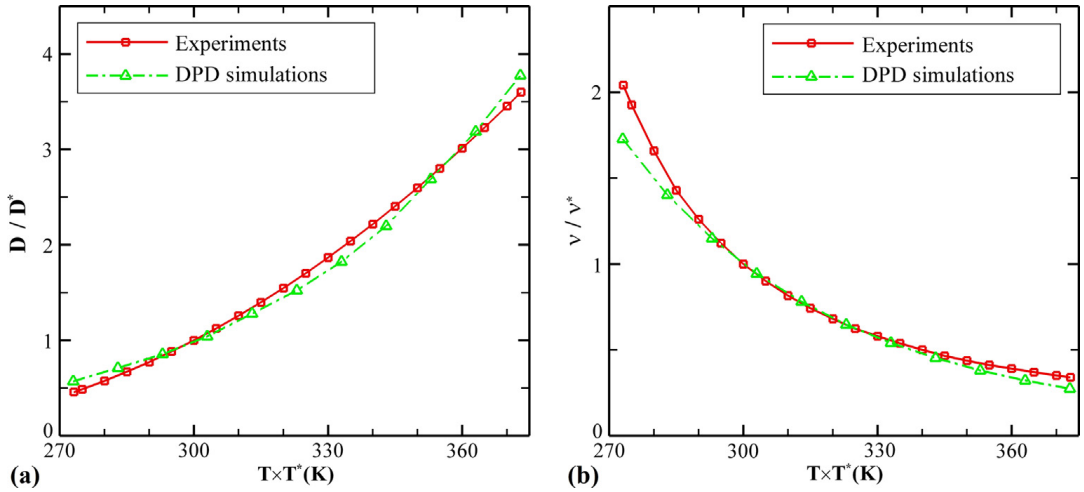

Fig. 10. Comparison of the temperature-dependent (a) diffusivity and (b) kinematic viscosity ranging from 273 K to 373 K between the experimental data of liquid water [18,30] and the results of eDPD simulations. Both the diffusivity and kinematic viscosity are scaled by their value at 300 K. For eDPD fluids, $D^* = 1.87 \times 10^{-2}$, $\upsilon^* = 6.62$ at $T = 1.00$ and the corresponding Schmidt number (Sc) is 354.01 comparable to Sc = 355.60 of liquid water at 300 K.

body-force applied on eDPD particles and $d = 15.00$ the half-length of the computational domain in z-direction. From the simulations we find $D = 1.87 \times 10^{-2}$, $\upsilon = 6.62$ at $T = 1.00$ and the corresponding Schmidt number is 354.01 comparable to the experimental data Sc = 355.60. Inserting the eDPD parameters in the approximate theoretical predictions Eqs. (10) and (11) give $D = 1.95 \times 10^{-2}$, $\upsilon = 6.45$ hence Sc = 331.33, which have errors less than 10% of the computed results. When the temperature of the eDPD system is increased, as expected, the diffusivity of the eDPD fluid increases as shown in Fig. 9(a) but the kinematic viscosity decreases as shown in Fig. 9(b). To test the performance of our non-isothermal model in the entire range of 273 K to 373 K, the temperature-dependent diffusivity and kinematic viscosity are computed by the same method as that used in Fig. 9, and the results are plotted in Fig. 10. Fig. 10(a) represents the comparison of the temperature-dependent diffusivity between the results of eDPD simulations and the experimental data of liquid water. It shows that the diffusivity is overestimated near 273 K and 373 K. However, the relative errors of diffusivity are less than 5% of experimental data for 290 K $< T \cdot T^* <$ 373 K. The temperature-dependent kinematic viscosity of eDPD fluid and the experimental data of liquid water are plotted in Fig. 10(b); it can be observed that the kinematic viscosity is underestimated near 273 K and 373 K. The relative errors of the kinematic viscosity of eDPD fluid are less than 10% of experimental data for 283 K $< T \cdot T^* <$ 353 K. The overestimation of diffusivity and underestimation of viscosity near 273 K and 373 K enlarge the errors in Schmidt number. Fig. 11 shows the comparison of Schmidt number between the eDPD fluid and the experimental data of liquid water. The relative error of Sc has its maximum 35% at 273 K and approximately 25% at 373 K, however, the relative errors are less than 10% of experimental data for 293 K $< T \cdot T^* <$ 353 K.

Overall, the proposed eDPD model reproduces the correct temperature-dependent dynamic properties including the diffusivity and the kinematic viscosity as well as Schmidt number comparable to the experimental data of liquid water for the

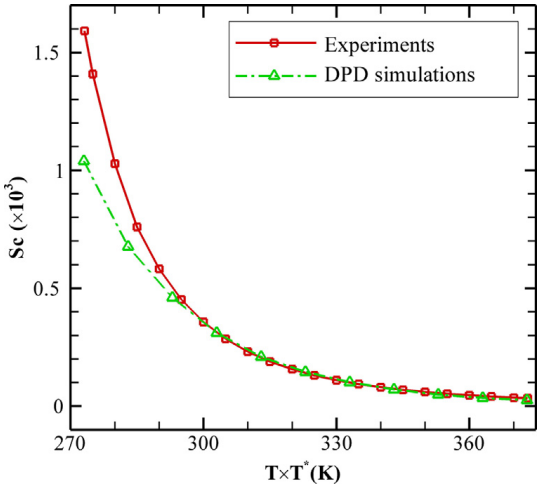

Fig. 11. Comparison of the temperature-dependent Schmidt number for the temperature ranging from 273 K to 373 K between the experimental data of liquid water [18,30] and the results of eDPD simulations.

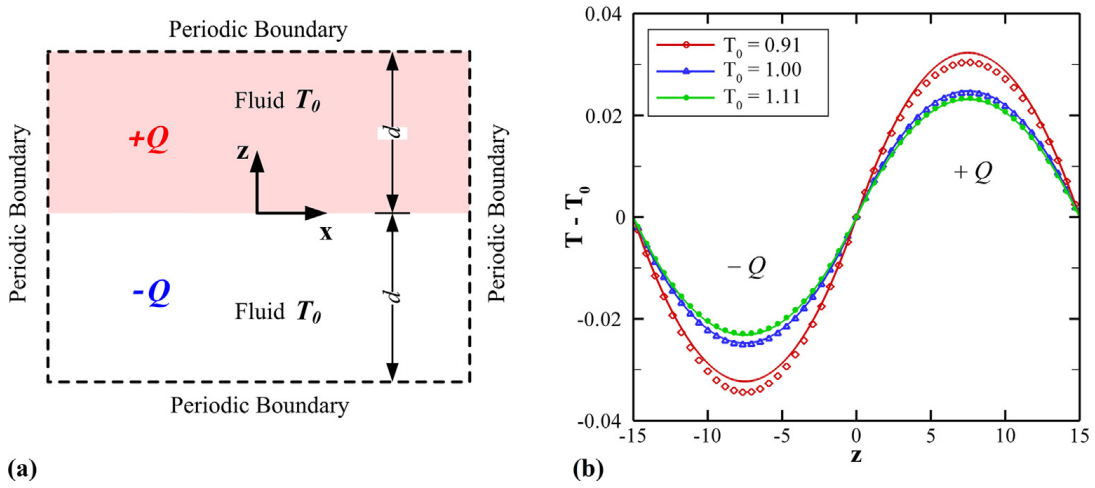

Fig. 12. (a) Schematic of the geometry for measuring the thermal conductivity by heat conduction analog of periodic Poiseuille flow. (b) Temperature profiles obtained using the heat conduction analog of periodic Poiseuille flow for different temperatures. The lines are quadratic solution given by Eq. (29) based on constant thermal diffusivity.

temperatures ranging from 273 K to 373 K. Although the diffusivity is overestimated and the viscosity is underestimated when the temperature approaches to 273 K and 373 K, the relative errors of these properties as well as Schmidt number are less than 10% of experimental data for 293 K $< T \cdot T^* <$ 353 K.

Similar to the diffusivity and viscosity, the thermal conductivity is also an output property instead of input parameter but it can be computed from other eDPD parameters such as C_v and κ according to Eq. (14). We proposed an analytical formula given by Eq. (15) for determining the mesoscopic heat friction κ but its validity has to be verified by measuring the thermal conductivity of the eDPD fluid. The heat conduction of a fluid is governed by the heat equation, which follows from the conservation of energy and it is given by:

$$\rho C_v \frac{\partial T}{\partial t} = \eta \nabla^2 T + \rho q, \tag{27}$$

where C_v is the specific heat, η the thermal conductivity and q the heat source. For steady state problems, the heat equation simplifies to

$$\lambda \nabla^2 T = -Q, \tag{28}$$

where λ is the thermal diffusivity given by $\lambda = \eta/\rho C_v$, and $Q = q/C_v$. By looking at the governing equation of heat conduction given by Eq. (28), it is noticed that Eq. (28) is the same as the governing equation of Poiseuille flow driven by gravitational force $\upsilon \nabla^2 \mathbf{V} = -g$, in which the kinematic viscosity υ and the gravitational force g are replaced by the thermal diffusivity λ and the heat source Q, respectively. Thus, we propose a heat conduction analog of periodic Poiseuille flow to compute the thermal conductivity of eDPD fluid, and this method for determining the thermal conductivity is not limited to eDPD but can be applied to other particle models as well.

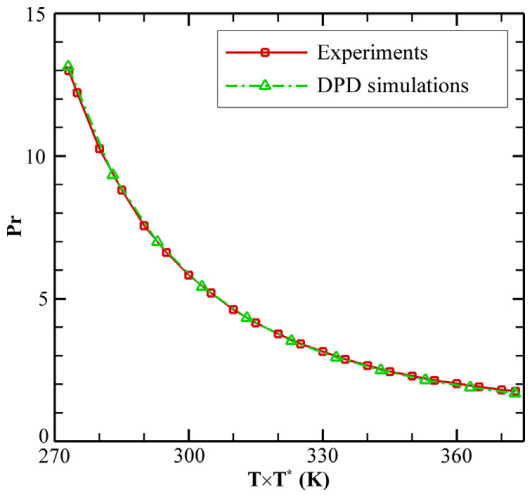

Fig. 13. Comparison of the temperature-dependent Prandtl number for the temperature ranging from 273 K to 373 K between the experimental data of liquid water and the results of eDPD simulations. The simulations are carried out in a computational domain of $30.0 \times 6.0 \times 30.0$ in DPD units with $\rho = 4.0$, $\alpha = 18.75 k_B T$, $\gamma = 4.5$, $r_C = 1.58$, $s = 0.41 + 1.9(T^2 - 1)$, $C_v = 1.0 \times 10^5$ and κ given by Eq. (15).

The heat conduction analog of periodic Poiseuille flow is obtained by applying a non-contact heat source such as microwave irradiation to each eDPD particle. For simplifying the simulation, a similar idea like in Ref. [31] for simulating periodic Poiseuille flow is adopted. The fluid system is subdivided into two domains in z-direction as described in Fig. 12(a), and a heat source $+Q$ is applied in upper domain while a heat sink with same magnitude $-Q$ is applied in lower domain. Because of the periodic boundary conditions the counteracting heat sources constrain the temperature of the eDPD fluid at the position where a plate with fixed temperature would be. For the geometry given by Fig. 12(a) the gradient of heat source in the x-direction vanishes so that the temperature is dependent on only z. With a constant thermal diffusivity λ the steady state solution of the heat conduction analog of periodic Poiseuille flow is given by:

$$T(z) = \frac{Q z}{2\lambda}\left(d - |z|\right) + T_0, \tag{29}$$

where T_0 is the temperature of the eDPD system before heating/cooling, d the half length of the computational domain in z-direction and λ the thermal diffusivity. Then, the value of thermal diffusivity λ at T_0 is computed by:

$$\lambda(T_0) = \frac{1}{2}(\lambda_+ + \lambda_-) = \frac{Q d^2}{16}\left(\frac{1}{T_{\max}} - \frac{1}{T_{\min}}\right), \tag{30}$$

where $T_{\max}$ is the maximum value of the temperature subtracting T_0 and $T_{\min}$ the minimum value subtracting T_0, λ_+ and λ_- are the thermal diffusivity calculated based on $T_{\max}$ and $T_{\min}$, respectively. The solid lines in Fig. 12(b) are symmetric parabolas given by Eq. (29) based on constant thermal diffusivity $\lambda(T_0)$. If the thermal diffusivity is constant and independent of the temperature, the amplitude of the temperature profile $|T_{\max}|$ on the right-hand side and $|T_{\min}|$ on the left-hand side should have the same value and the computed temperature profiles should coincide with the solid lines. However, the thermal diffusivity of the fluid is temperature-dependent and variable along the z direction. For $z < 0$ the temperature of the eDPD fluid is smaller than T_0 due to the heat sink, and the fluid has smaller thermal diffusivity λ_-, thus the computed temperature profile is lower than the solid line. In contrast, for $z > 0$ the temperature of the eDPD fluid is larger than T_0 due to the heat source, and the fluid has larger thermal diffusivity λ_+, thus the computed temperature profile is also lower than the solid line. That is why a shift in the temperature profile is observed in Fig. 12(b). Considering a small variation of the temperature, both λ_+ and λ_- are close to $\lambda(T_0)$ and the value of $\lambda(T_0)$ can be approximated by the average of λ_+ and λ_-. In the present work, a small heat source $Q = q/C_v = 1.0 \times 10^{-3}$ is used to avoid large variation of the temperature. The mesoscopic heat friction κ is given by Eq. (15) with the computed kinematic viscosity and other eDPD parameters the same as these used in Section 3.3.

The temperature profiles shown in Fig. 12(b) were obtained by subdividing the computational domain into 51 bins along z-direction, while the simulations were run for 500 time units and the results were averaged over the last 100 time units. It can be observed that the computed temperature profiles in Fig. 12(b) are lower than the analytical solution of Eq. (29) with constant λ because of the variation of thermal diffusivity λ. The change of the temperature is controlled within 5% of the system temperature T_0 shown in Fig. 12(b). The three curves of $T_0 = 0.91$, 1.00 and 1.11 in Fig. 12(b) give $\lambda_+ = 0.92$, 1.15, 1.23 and $\lambda_- = 0.82$, 1.12, 1.20, hence the computed thermal diffusivity for each case is $\lambda = 0.870$, 1.135 and 1.215, respectively.

Using the heat conduction analog of periodic Poiseuille flow the thermal diffusivity of eDPD fluid ranging from 273 K to 373 K was computed, and the result is represented by Prandtl number $Pr = \upsilon/\lambda$, which is the ratio of momentum diffusivity (kinematic viscosity) υ to thermal diffusivity λ. Fig. 13 displays the comparison of the temperature-dependent

Prandtl number between the results of eDPD simulations and the experimental data of liquid water. It can be observed that the Prandtl numbers of eDPD fluid are consistent with the experimental Prandtl numbers. The relative error is less than 5% of experimental Pr for the entire temperature range of 273 K to 373 K, which verifies the analytical formula of Eq. (15) for determining the mesoscopic heat friction. It is worth noting that Eq. (15) for determining the mesoscale heat friction κ is obtained based on a rough assumption of $g(r) = 1.0$. By using the computed kinematic viscosity the result in Fig. 13 reveals that Eq. (15) leads to good accuracy for liquid water ranging from 273 K to 373 K even without any correction for $g(r)$.

4. Summary and discussion

An energy-conserving dissipative particle dynamics (eDPD) model for reproducing correctly the temperature-dependent properties including Schmidt number and Prandtl number has been proposed. The relationships between the dynamic properties of eDPD fluid and the parameters in the dissipative and random forces have been analyzed. The exponent of the weighting function was properly chosen as a temperature-dependent variable. To eliminate the effect from the density fluctuations at the wall boundaries, we replaced the real solid wall by effective boundary forces and heat fluxes, which are extracted from the fluid–solid interactions using the continuum approximation. Simulations of a time-dependent planar Poiseuille flow and a steady-state heat conduction for reproducing the Fourier law were carried out to validate the present eDPD formulation and the new method for imposing thermal boundary conditions.

The diffusivity and viscosity of liquid water at various temperatures ranging from 273 K to 373 K were used as a benchmark for verifying the model. The results showed that the present model reproduces the correct temperature-dependent properties including diffusivity and kinematic viscosity consistent with the available experimental data of liquid water. Moreover, an analytical formula for determining the mesoscopic heat friction has been proposed. The validity of the formula is confirmed by reproducing the experimental data for Prandtl number of liquid water at various temperatures.

Hence, this work proposes a non-isothermal DPD model which is able to reproduce the correct temperature-dependent Schmidt numbers and Prandtl numbers, and a method to impose thermal boundary conditions with effective boundary forces and heat fluxes so that the density fluctuation in the vicinity of the boundary can be effectively eliminated. In particular, we proposed a methodology to determine the mesoscopic heat friction based on experimental measurements instead of empirical parameters. Although we test our model with liquid water, the method proposed in the present work for modeling the correct temperature-dependent properties is not limited to water only and it can be readily extended to other fluids.

The traditional DPD framework considers only the dissipative and random forces along the inter-particle axis. Pan et al. [32] and Junghans et al. [33] employed the transverse DPD thermostat to include the non-central dissipative and random forces, see also the analysis of Lei et al. [34]. The transverse DPD thermostat can be also applied in the non-isothermal DPD model when the heat flux contributed by viscous heating is correctly modeled, which would be interesting for further research. However, it is worth noting that the non-central forces should be coupled with the rotation of particles to account for the conservation of angular momentum of the system.

Acknowledgements

This work was primarily sponsored by the Army Research Laboratory and was accomplished under Cooperative Agreement Number W911NF-12-2-0023 to University of Utah and partially supported by the new DOE Center on Mathematics for Mesoscopic Modeling of Materials (CM4). Computations were performed at the IBM BG/P with computer time provided by an INCITE grant.

References

[1] P.J. Hoogerbrugge, J.M.V.A. Koelman, Simulating microscopic hydrodynamic phenomena with dissipative particle dynamics, Europhys. Lett. 19 (3) (1992) 155–160.
[2] X.J. Fan, N. Phan-Thien, S. Chen, X.H. Wu, T.Y. Ng, Simulating flow of DNA suspension using dissipative particle dynamics, Phys. Fluids 18 (6) (2006) 063102.
[3] S. Litvinov, M. Ellero, X.Y. Hu, N.A. Adams, Smoothed dissipative particle dynamics model for polymer molecules in suspension, Phys. Rev. E 77 (6) (2008) 066703.
[4] V. Symeonidis, G.E. Karniadakis, B. Caswell, Dissipative particle dynamics simulations of polymer chains: Scaling laws and shearing response compared to DNA experiments, Phys. Rev. Lett. 95 (7) (2005) 076001.
[5] D.A. Fedosov, B. Caswell, G.E. Karniadakis, A multiscale red blood cell model with accurate mechanics, rheology, and dynamics, Biophys. J. 98 (10) (2010) 2215–2225.
[6] D.A. Fedosov, B. Caswell, S. Suresh, G.E. Karniadakis, Quantifying the biophysical characteristics of plasmodium-falciparum-parasitized red blood cells in microcirculation, Proc. Natl. Acad. Sci. USA 108 (1) (2011) 35–39.
[7] I.V. Pivkin, P.D. Richardson, G.E. Karniadakis, Effect of red blood cells on platelet aggregation, IEEE Eng. Med. Biol. Mag. 28 (2) (2009) 32–37.
[8] Z. Li, G.H. Hu, Z.L. Wang, Y.B. Ma, Z.W. Zhou, Three dimensional flow structures in a moving droplet on substrate: A dissipative particle dynamics study, Phys. Fluids 25 (7) (2013) 072103.
[9] P. Espanol, P. Warren, Statistical mechanics of dissipative particle dynamics, Europhys. Lett. 30 (4) (1995) 191–196.
[10] P. Espanol, Dissipative particle dynamics with energy conservation, Europhys. Lett. 40 (6) (1997) 631–636.
[11] M. Ripoll, P. Espanol, M.H. Ernst, Dissipative particle dynamics with energy conservation: Heat conduction, Int. J. Mod. Phys. C 9 (8) (1998) 1329–1338.
[12] R. Qiao, P. He, Simulation of heat conduction in nanocomposite using energy-conserving dissipative particle dynamics, Mol. Simul. 33 (8) (2007) 677–683.

[13] E. Abu-Nada, Natural convection heat transfer simulation using energy conservative dissipative particle dynamics, Phys. Rev. E 81 (5) (2010) 056704.
[14] P. He, R. Qiao, Self-consistent fluctuating hydrodynamics simulations of thermal transport in nanoparticle suspensions, J. Appl. Phys. 103 (9) (2008) 094305.
[15] A.D. Mackie, J.B. Avalos, V. Navas, Dissipative particle dynamics with energy conservation: Modelling of heat flow, Phys. Chem. Chem. Phys. 1 (9) (1999) 2039–2049.
[16] S.M. Willemsen, H.C.J. Hoefsloot, D.C. Visser, P.J. Hamersma, P.D. Iedema, Modelling phase change with dissipative particle dynamics using a consistent boundary condition, J. Comput. Phys. 162 (2) (2000) 385–394.
[17] R.D. Groot, P.B. Warren, Dissipative particle dynamics: Bridging the gap between atomistic and mesoscopic simulation, J. Chem. Phys. 107 (11) (1997) 4423–4435.
[18] T.L. Bergman, A.S. Lavine, F.P. Incropera, D.P. DeWitt, Introduction to Heat Transfer, 6th edition, John Wiley and Sons, 2011.
[19] I.V. Pivkin, G.E. Karniadakis, A new method to impose no-slip boundary conditions in dissipative particle dynamics, J. Comput. Phys. 207 (1) (2005) 114–128.
[20] E. Abu-Nada, Energy conservative dissipative particle dynamics simulation of natural convection in liquids, ASME J. Heat Transf. 133 (11) (2011) 112502.
[21] E. Abu-Nada, Heat transfer simulation using energy conservative dissipative particle dynamics, Mol. Simul. 36 (5) (2010) 382–390.
[22] C.A. Marsh, G. Backx, M.H. Ernst, Fokker–Planck–Boltzmann equation for dissipative particle dynamics, Europhys. Lett. 38 (6) (1997) 411–415.
[23] J.B. Avalos, A.D. Mackie, Dynamic and transport properties of dissipative particle dynamics with energy conservation, J. Chem. Phys. 111 (11) (1999) 5267–5276.
[24] D. Duong-Hong, N. Phan-Thien, X.J. Fan, An implementation of no-slip boundary conditions in DPD, Comput. Mech. 35 (1) (2004) 24–29.
[25] S.M. Willemsen, H.C.J. Hoefsloot, P.D. Iedema, No-slip boundary condition in dissipative particle dynamics, Int. J. Mod. Phys. C 11 (5) (2000) 881–890.
[26] S.K. Ranjith, B.S.V. Patnaik, S. Vedantam, No-slip boundary condition in finite-size dissipative particle dynamics, J. Comput. Phys. 232 (1) (2013) 174–188.
[27] H. Lei, D.A. Fedosov, G.E. Karniadakis, Time-dependent and outflow boundary conditions for dissipative particle dynamics, J. Comput. Phys. 230 (10) (2011) 3765–3779.
[28] L.D.G. Sigalotti, J. Klapp, E. Sira, Y. Melean, A. Hasmy, SPH simulations of time-dependent Poiseuille flow at low Reynolds numbers, J. Comput. Phys. 191 (2) (2003) 622–638.
[29] S. Plimpton, Fast parallel algorithms for short-range molecular dynamics, J. Comput. Phys. 117 (1) (1995) 1–19.
[30] M. Holz, S.R. Heil, A. Sacco, Temperature-dependent self-diffusion coefficients of water and six selected molecular liquids for calibration in accurate H-1 NMR PFG measurements, Phys. Chem. Chem. Phys. 2 (20) (2000) 4740–4742.
[31] J.A. Backer, C.P. Lowe, H.C.J. Hoefsloot, P.D. Iedema, Poiseuille flow to measure the viscosity of particle model fluids, J. Chem. Phys. 122 (15) (2005) 154503.
[32] W. Pan, I.V. Pivkin, G.E. Karniadakis, Single-particle hydrodynamics in DPD: A new formulation, Europhys. Lett. 84 (1) (2008) 10012.
[33] C. Junghans, M. Praprotnik, K. Kremer, Transport properties controlled by a thermostat: An extended dissipative particle dynamics thermostat, Soft Matter 4 (1) (2008) 156–161.
[34] H. Lei, B. Caswell, G.E. Karniadakis, Direct construction of mesoscopic models from microscopic simulations, Phys. Rev. E 81 (2) (2010) 026704.